Int. J. Heat Mass Transfer. Vol. 30, No. 6, pp. 1169–1182, 1987
Printed in Great Britain

0017–9310/87 $3.00 + 0.00

Effect of channel geometry on critical heat flux for low pressure water

KAICHIRO MISHIMA and HIDEAKI NISHIHARA
Research Reactor Institute, Kyoto University, Kumatori-cho, Sennan-gun, Osaka 590-04, Japan

(*Received* 20 *September* 1985 *and in final form* 30 *April* 1986)

Abstract—The main difficulty in interpreting critical heat flux (CHF) at low velocity and pressure conditions arises from the fact that the burnout phenomenon under such conditions is vulnerable to the effect of buoyancy and flow instabilities. This study is intended to provide some systematic understanding on CHF at low velocity and pressure conditions. Data obtained in the previous experiments for water in an annulus, rectangular ducts and a round tube are briefly reviewed and augmented in collaboration with existing data and correlations to extract more generic information. The effect of channel geometry on CHF is then discussed. The effect of channel geometry turned out to be remarkable at intermediate mass velocities. The difference in CHF at these mass velocities between a round tube and the other channel geometries was attributed mainly to the existence of an unheated wall which cause a non-uniform distribution of liquid film.

1. INTRODUCTION

THE IMPORTANCE of critical heat flux (CHF) data for water at low velocity and pressure conditions has been pointed out earlier [1, 2] in relation to the loss-of-coolant accident (LOCA) characteristics of low velocity, flow stagnation and flow reversal. It is known that the burnout phenomenon at low velocity and pressure conditions is complicated because the effect of buoyancy becomes remarkable at low velocities and the flow becomes less stable at low pressures. This, in fact, has been a main difficulty in interpreting CHF at low pressures systematically.

Recently, Mishima and co-workers performed low-flow CHF experiments for water at atmospheric pressure employing three different channel geometries, i.e. an annulus [3], rectangular ducts [4] and a round tube [5]. The dimensions of the channels are shown in Table 1. The experiments were conducted with a test rig as shown in Fig. 1. Ion-exchanged water flowed through the test section and the heater (stainless-steel tube or plate) was directly Joule heated. The test section was kept at about atmospheric pressure.

In the annulus and rectangular ducts, the flow regime at the occurrence of burnout was visually observed and the CHF was measured. In the experiment with the round tube test section, more emphasis was placed on the effect of flow instability on CHF. The difference in CHF between upflow and downflow was also investigated for the rectangular ducts and the round tube test section [4, 5].

In the present study, the results for each channel geometry are briefly reviewed and augmented in collaboration with existing data and correlations to find more generic conclusions. The effect of channel geometry is then discussed.

2. EQUATIONS PERTINENT TO CHF

When a heated wall is submerged in a pool of water, pool-boiling CHF occurs due to departure from nucleate boiling (DNB) at an excessive high heat flux despite sufficient ambient liquid. Kutateladze [6] interpreted pool-boiling CHF as a hydrodynamic phenomenon. Based upon a non-linear Euler equation of motion and energy equation, and making use of a dimensional analysis, he obtained the following dimensionless correlation for pool-boiling CHF:

$$q^*_{cP} = q_{cP}/[h_{fg}(\rho_g^2 \sigma g \Delta\rho)^{1/4}] = \text{const.} \quad (1)$$

Zuber [7] also arrived at the same equation theoretically considering hydrodynamic instabilities which occur above a heated horizontal wall. The constant on the right-hand side ranges from 0.13 to 0.19 depending upon the geometry of the heated wall.

On the basis of the above equation, CHF data are plotted in terms of dimensionless heat flux q^* and mass velocity G^* defined by

$$q^* = q/(h_{fg}\sqrt{(\lambda \rho_g g \Delta\rho)}) \quad (2)$$

$$G^* = G/\sqrt{(\lambda \rho_g g \Delta\rho)} \quad (3)$$

where the length scale λ of the Taylor instability is given by

$$\lambda = \sqrt{(\sigma/(g\Delta\rho))}. \quad (4)$$

The dimensionless expression in equation (2) is equivalent to that in equation (1).

When liquid flows through a heated channel, mismatching between the liquid circulation and the heat input can cause a burnout or dryout of the heated wall. Let Δh_i be the liquid enthalpy subcooling at the

NOMENCLATURE

A	flow area
A_H	heated area
C	constant in the Wallis correlation for flooding
C_0	distribution parameter given by equation (12) or equation (13)
D	tube diameter or characteristic length
D^*	dimensionless tube diameter, equation (8)
D_H	heated equivalent diameter
D_i	diameter of the inner wall
D_o	diameter of the outer wall
G	mass velocity
G^*	dimensionless mass velocity, equation (3)
G_c	critical mass velocity to stagnate bubbles, equation (11)
g	gravity
h_{fg}	latent heat of evaporation
Δh_i	inlet enthalpy subcooling
L	heated length
P	pressure
q	heat flux
q_{cF}	flooding CHF
q_{cP}	pool-boiling CHF
q^*	dimensionless heat flux, equation (2)
q^*_{cF}	dimensionless CHF due to flooding
q^*_{cL}	dimensionless CHF in the Katto L-regime
q^*_{cP}	dimensionless pool-boiling CHF
s	gap of annulus or rectangular duct
T_{in}	inlet water temperature
w	width (wider span) of a rectangular duct
x_e	exit equilibrium quality
x_{ec}	critical quality
x_{eR}	critical quality obtained from the Katto L-regime correlation.

Greek symbols

ζ	parameter for flooding CHF correlation
λ	length scale of the Taylor wave
ξ	wetted perimeter
ξ_H	heated perimeter
ρ_k	density of k phase (k = g or l)
$\Delta\rho$	difference of the density between two phases
σ	surface tension.

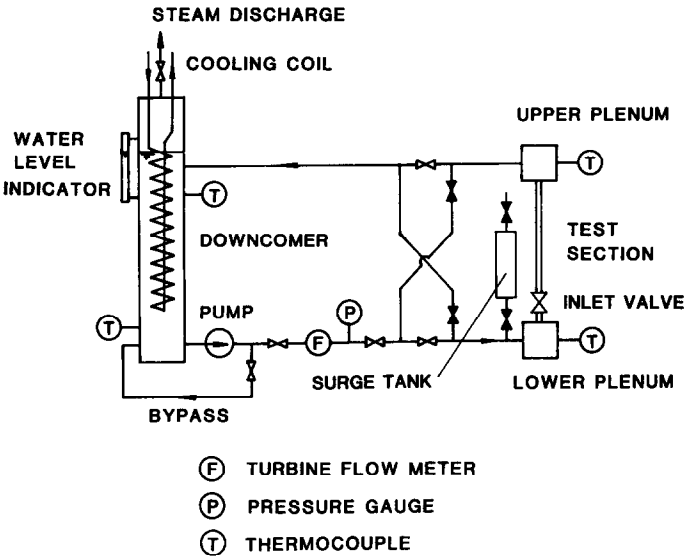

FIG. 1. Schematic diagram showing the test rig employed in previous studies.

inlet and x_e the exit quality, then the energy balance equation in the heated section gives the following relation between q^* and G^*:

$$q^* = \frac{A}{A_H}\left(x_e + \frac{\Delta h_i}{h_{fg}}\right)G^*. \quad (5)$$

Although the gravity term is included in the dimensionless group q^* and G^*, the CHF in this case does not depend upon it, because the gravity term is cancelled out if the equation is rewritten as follows:

$$\text{Boiling number} = \frac{q}{h_{fg}G} = \frac{q^*}{G^*} = \frac{A}{A_H}\left(x_e + \frac{\Delta h_i}{h_{fg}}\right). \quad (6)$$

In this sense, use of the boiling number may be more appropriate for a dimensionless group when the effect of gravity is not important. Nevertheless, we use here the q^*–G^* coordinate scheme since our objective is to

Table 1. Dimensions of the test sections employed in the previous experiments

	Internally heated annulus [3]	Rectangular ducts [4]		Round tube [5]
		Heated from one side	Heated from two sides	
Dimensions of the cross-section (mm)	$D_i = 20.45$ $D_o = 25.96$	2.4×40 $\xi_H = 30.0$	2.4×40 $\xi_H = 60.0$	$D = 6.0$
Heated length L (cm)	59.69	35.0	35.0	34.4
Flow area A (cm^2)	2.008	0.96	0.96	0.283
Heated area A_H (cm^2)	383.5	105.0	210.0	64.8
Hydraulic diameter D (mm)	5.509	4.528	4.528	6.0

observe changes in CHF as a function of the mass velocity among different channel geometries.

When $x_e = 1$, all the liquid entering the heated section is evaporated and dryout occurs at the outlet. Thus CHF is limited by liquid circulation. In reality, burnout occurs due to dryout or breakup of liquid film in the annular flow regime. The CHF in this case is usually close to the condition given by equation (5) with $x_e = 1$ at relatively low flow rates where liquid entrainment is not much. This is called, therefore, high-quality CHF. When the mass velocity and the heat flux is high, the amount of liquid entrainment increases and accordingly the flow rate in the liquid film decreases. Then, the CHF becomes lower. This is called entrainment-limited CHF.

At the boiling condition with the bottom end closed, one may observe a countercurrent flow, i.e. the vapor flows up from the heated section while the liquid falls down from the upper plenum due to gravity. When the heat input is sufficiently large, the vapor flow causes countercurrent-flow limitation (CCFL) or flooding at the top, which leads to a liquid deficiency in the heated section. Hence the CHF is limited by flooding, which we call flooding CHF. Flooding CHF is estimated approximately by using the Wallis correlation [8] together with the energy balance equation. Therefore

$$q_{cF} = \frac{A}{A_H} \cdot \frac{C^2 h_{fg} \sqrt{(\rho_g g \Delta\rho D)}}{[1 + (\rho_g/\rho_l)^{1/4}]^2}. \quad (7)$$

In equation (7), the constant C depends upon the geometry of the test section and is determined empirically. It has been pointed out also that the constant C includes the effect of surface tension which is expressed in terms of the dimensionless hydraulic diameter D^* [9]

$$D^* = D/\lambda. \quad (8)$$

Therefore, it may not be unreasonable to write equation (7) in a dimensionless form which includes D^*. Using equations (2)–(4) and (8), the following equation is obtained:

$$q^*_{cF} = \frac{A}{A_H} \cdot \frac{C^2 \sqrt{D^*}}{[1 + (\rho_g/\rho_l)^{1/4}]^2}. \quad (9)$$

Usually the flooding CHF is much lower than the pool-boiling CHF given by equation (1). When the length-to-diameter ratio L/D is small, however, the flooding CHF approaches the pool-boiling CHF.

It probably occurs in upflow at a certain low mass velocity and a heat flux that even when all the liquid entering from the bottom is evaporated until it reaches the outlet, liquid can fall down from the upper plenum and a countercurrent flow arises in the upper portion of the heated section. The CHF is then limited by liquid circulation and flooding [3].

It was observed in the experiment with an annular test section [3] that dry patches on the heated surface were quenched by the passage of liquid bridges in the churn flow regime. Burnout occurred, however, due to dryout of liquid film just after the flow regime changed from churn flow to annular flow. The condition for this flow regime transition was obtained by Mishima and Ishii [10]. The approximate equation for the boundary between those flow regimes in a low pressure system is expressed in terms of q^* and G^* as follows:

$$q^* = q^*_{cF} + \frac{A}{A_H} \cdot \frac{\Delta h_i}{h_{fg}} G^*. \quad (10)$$

The first term is equal to the flooding CHF, equation (9). The second one is the heat required to bring subcooled liquid to saturation which is obtained from equation (5) with the condition $x_e = 0$. It is seen, therefore, that the annular-flow boundary given by equation (10) approaches flooding CHF at very low mass velocities, whereas the boundary comes close to equation (5) with the condition $x_e = 0$ at high mass velocities.

3. EXISTING DATA AND CORRELATIONS

3.1. *CHF in annuli*

In the previous study [3], CHF at relatively low mass velocities has been investigated. The results are shown in Fig. 2. They are compared with equations (1), (5), (9) and (10) as well as with existing correlations for high-quality CHF. The Katto correlation scheme [11] and the Barnett correlation [12] are employed as

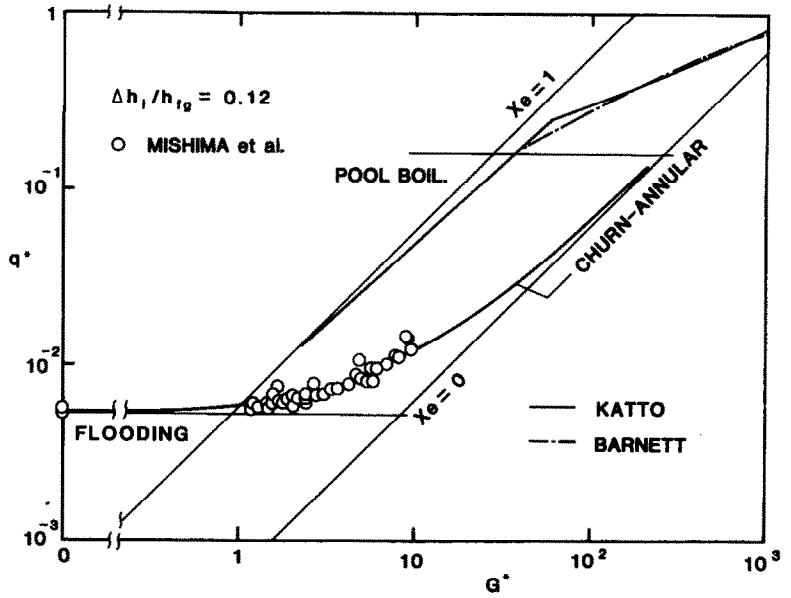

FIG. 2. CHF for upflow at low mass velocities in an internally heated annulus [3].

the high-quality CHF correlations. The Katto correlation scheme consists of two correlations, i.e. L-regime and H-regime correlations. The former corresponds to the high-quality CHF and the latter to the entrainment-limited CHF or CHF due to flow instability

Figure 2 indicates that the CHF at low mass velocities is much lower than the high-quality CHF and is correlated well by the annular flow boundary equation (10). The CHF at stagnant flow and very low mass velocities approaches flooding CHF which is predicted by equation (9) with $C = 0.8$. In Fig. 2, CHF data due to flooding fall in the region where the exit quality is larger than unity. The reason for this is that the exit quality is calculated based only upon the inlet mass velocity and the heat balance, and consequently the amount of liquid falling down from the upper plenum is not taken into account.

Since the tested ranges of the parameters in the previous study are limited, the data are supplemented by other available data from other sources [13, 14]. They are compared with the above equations and correlations in the same manner as shown in Fig. 2. The comparison is also made with the subcooled-boiling CHF correlation, for example the Zenkevich correlation [15].

CHF data for low pressure water in annular test sections ($D_i = 13.1$ mm, $D_o = 22$, 25, 30.2 mm, $L = 480$ mm) were obtained also by Rogers *et al.* [13]. Their data at high mass velocities as well as low mass velocities are shown in Figs. 3 and 4. They include data of CHF in the subcooled region.

It can be seen from these figures that their result at low mass velocities is consistent with those in Fig. 2 and that the CHF at higher mass velocities in the subcooled region is correlated reasonably well by the subcooled-boiling CHF. Figure 4 shows the data for small L/D_H, in which case the flooding CHF approaches the pool-boiling CHF. It should be noted that most of the data are plotted in the region where the churn or slug flow regime is predicted, which is consistent with the observation by Rogers *et al.* [13].

Another set of CHF data is available from a report prepared by the Japanese Society of Mechanical Engineers (*JSME*) [14]. The experiments were performed independently at several universities and institutions with a test section of the same design ($D_i = 10$ mm, $D_o = 19$ mm, $L = 300$ mm). The results at inlet water temperatures 95, 85 and 70°C are shown in Figs. 5, 6 and 7, respectively.

It is observed in Fig. 5 that the CHF data are divided into two groups, i.e. higher CHF data and lower CHF data at a given range of flow rate, although they were obtained under apparently the same conditions. The lower CHF data fall along the annular-flow boundary, whereas the higher CHF data are in the middle of the annular flow region. The discrepancy between the two groups was not interpreted satisfactorily. It was pointed out [14], however, that flow instability had been probably involved in the lower CHF data. Loop characteristics, such as inlet throttling and pump characteristics may have varied even in the same test loop.

Figure 6 shows the data in the intermediate region between the subcooled-boiling CHF and the CHF in the annular-flow regime. Figure 7 shows that the data in the subcooled-boiling region are well reproduced by the Zenkevich correlation [15].

Looking at Figs. 2–7, it is suggested that a change in burnout mechanism occurs when the exit quality is near zero. At such a condition, a small change in flow rate, heat flux, inlet subcooling, etc. causes either rapid formation or collapse of bubbles. The flow pattern

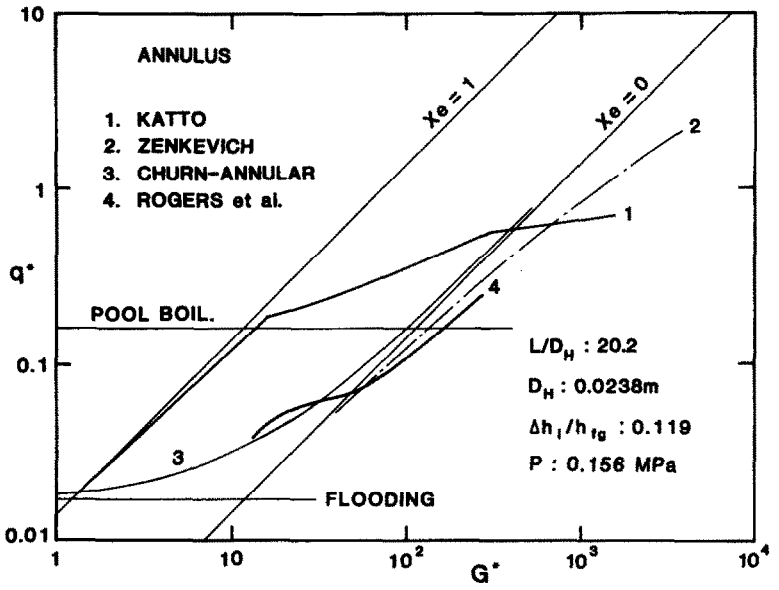

FIG. 3. CHF data of Rogers *et al.* [13] for upflow in an internally heated annulus.

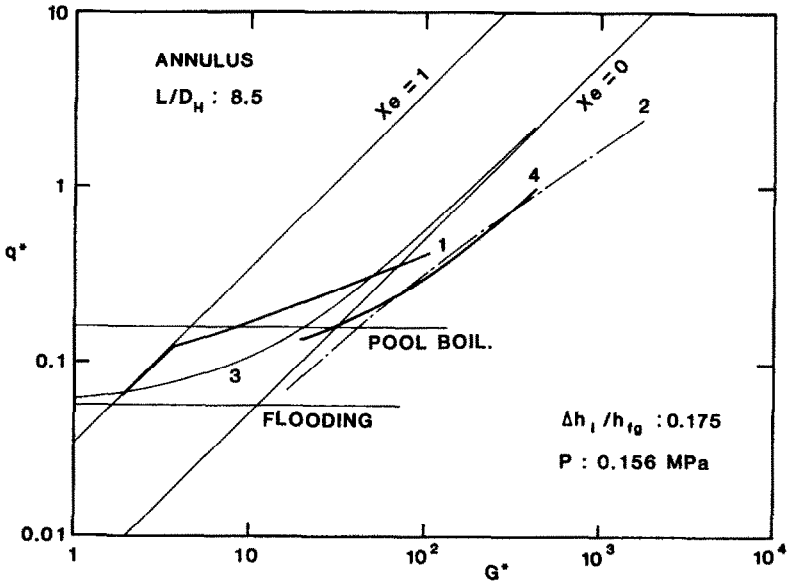

FIG. 4. CHF data of Rogers *et al.* [13] for upflow in an internally heated annulus with small L/D_H (legend as shown in Fig. 3 unless otherwise stated).

(two-phase flow regimes and the stability of the flow) varies quickly. The burnout process changes as a consequence.

3.2. *CHF in rectangular ducts*

3.2.1. *Upflow.* Figure 8 shows the results for a rectangular duct heated from one side [4]. The data are compared with equations (1), (5), (9) and (10) as well as high-quality CHF correlations (the Katto correlation scheme [16] and the Macbeth correlation [17]), and subcooled-boiling CHF correlations (the Mirshak correlation [18], the Labuntsov correlation [19] and the Kutateladze correlation [20]). The Mirshak correlation [18] was developed originally based upon data for downflow.

The results for upflow are summarized as follows:

(1) A minimum in CHF is observed at flow stagnation with the bottom end closed, where burnout occurs due to flooding. The minimum CHF can be calculated using equation (9) with $D = 2w$ and $C = 0.73$.

(2) At intermediate mass velocities, CHF increases along the line with approximately constant exit quality which we call the critical quality. The CHF with a constant critical quality lies in the region between the

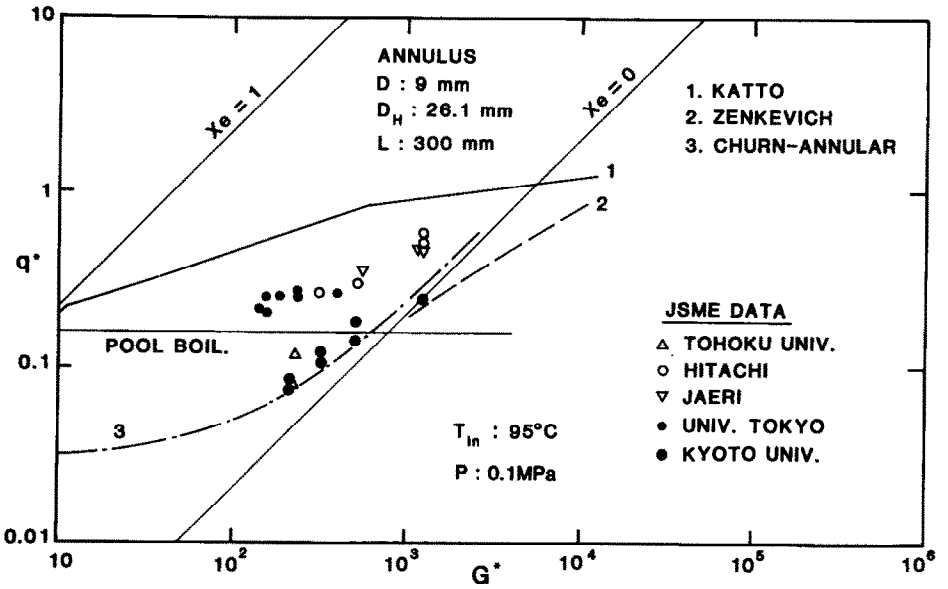

FIG. 5. CHF data of JSME [14] for upflow in an internally heated annulus at inlet water temperature 95°C.

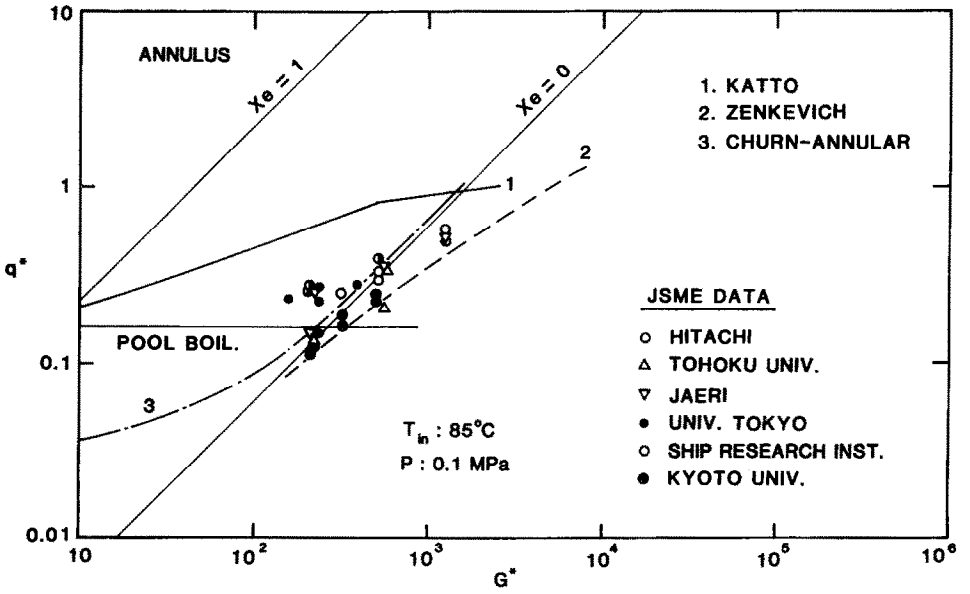

FIG. 6. CHF data of JSME [14] for upflow in an internally heated annulus at inlet water temperature 85°C.

high-quality CHF as an upper limit and the annular-flow boundary as a lower limit. In this case, burnout occurs due to liquid-film dryout in the annular flow regime.

(3) It is known that the subcooled-boiling CHF correlations [18–20] are appropriate in the subcooled region at high mass velocities. Therefore, it is deduced that the CHF curve would merge with those curves at high mass velocities.

3.2.2. *Downflow.* Figure 8 exhibits the data for downflow as well. The results are summarized as follows [4]:

(1) Burnout occurs due to flooding at low mass velocities less than the critical value to stagnate steam bubbles in the heated channel. Resultant CHF is minimum. The critical mass velocity for bubble stagnation is calculated based upon the drift flux model [21] and is given by

$$G_c = -\sqrt{2(\rho_l^2 \sigma g \Delta\rho)^{1/4}}/C_0 \tag{11}$$

where the negative sign means downflow. The distribution parameter C_0 is given by [21]

$$C_0 = 1.2 - 0.2\sqrt{(\rho_g/\rho_l)} \tag{12}$$

for annuli and round tubes, and

$$C_0 = 1.35 - 0.35\sqrt{(\rho_g/\rho_l)} \tag{13}$$

for rectangular ducts.

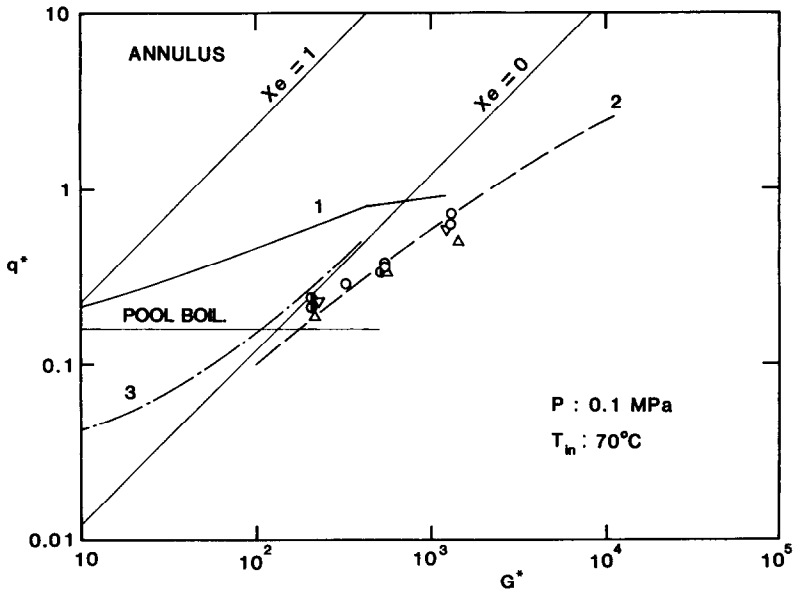

FIG. 7. CHF data of JSME [14] for upflow in an internally heated annulus at inlet water temperature 70°C (legend as shown in Fig. 6 unless otherwise stated).

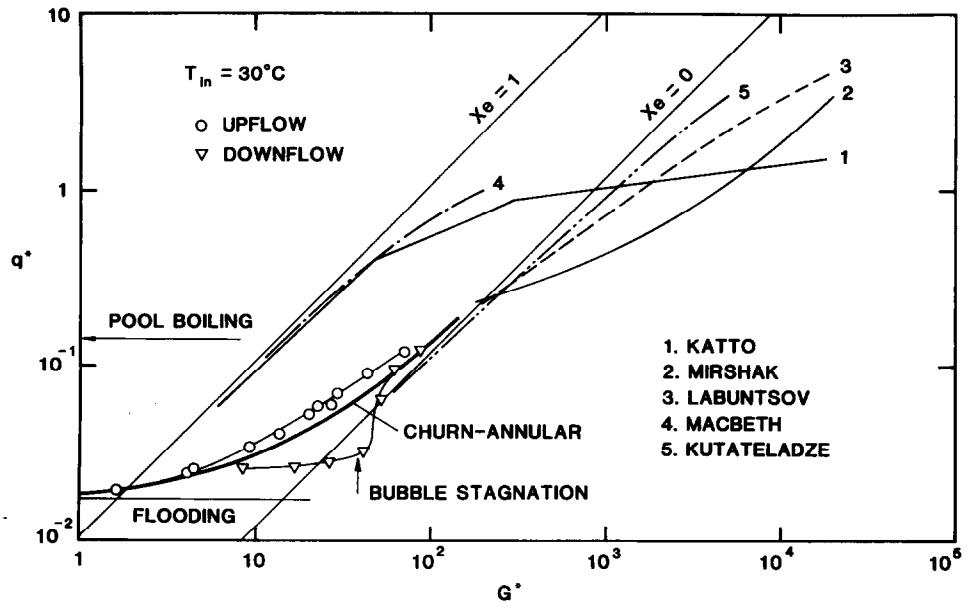

FIG. 8. CHF for upflow and downflow in a rectangular channel heated from one side [4].

(2) At intermediate mass velocities beyond the critical mass velocity G_c, burnout occurs at about zero exit quality. In this region, vigorous flow oscillations arise whose amplitude increases with increasing mass velocity and heat flux. The upper plenum may have worked as an energy storage mechanism to excite flow oscillations. Due to flow instability, CHF decreases substantially.

3.3. *CHF in round tubes*

3.3.1. *Upflow.* Figure 9 shows an example of CHF data obtained in the previous study for low-pressure water in a round tube [5]. Since the effects of the upper and lower plena and the inlet restriction are studied in the experiment, the loop conditions are also shown in the figure. The 'stiff' condition means that the bypass was closed and the inlet restriction was large, whereas the 'soft' condition means that the inlet valve was fully open and the bypass was open halfway (see Fig. 1). Thus the flow is more stable in a 'stiff' system. In this sense, the flow condition in the above mentioned experiment with an annulus and rectangular ducts is 'soft'.

The results are compared with equations (1), (5), (9) and (10) as well as with high-quality CHF correlations

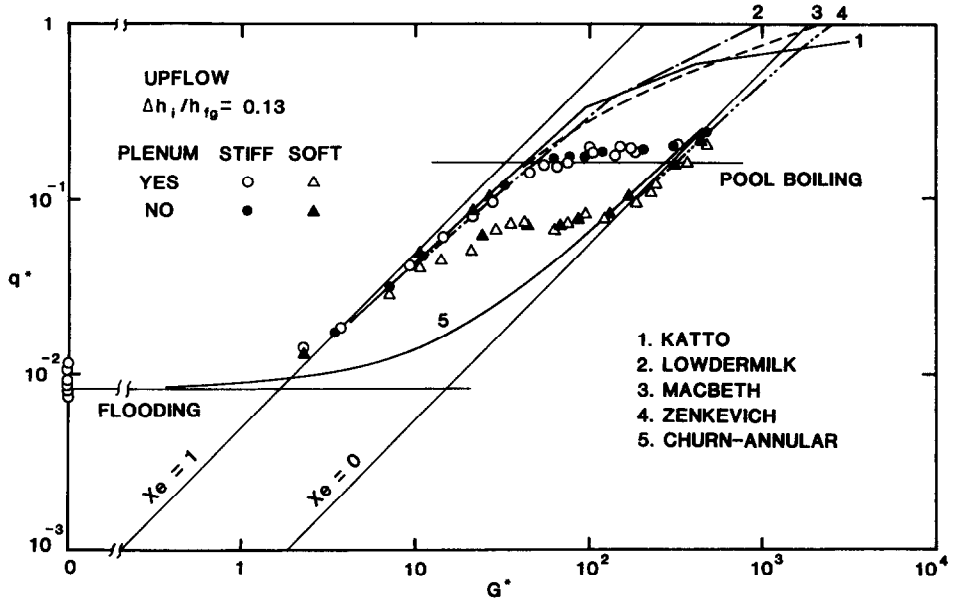

FIG. 9. CHF for upflow in a round tube [5].

(the Macbeth correlation [17]), the Katto correlation scheme [22] and the Lowdermilk correlation [23]), and a subcooled-boiling CHF correlation (the Zenkevich correlation [15]).

Although no visual observation was made in the experiment with the round tube, we will refer to the minimum CHF as 'flooding CHF', i.e. q^*_{cF} because of the similarity in the behavior of CHF. The minimum CHF then can be reproduced by equation (9) if we use the empirical value of $C = 1.66$, which is much larger than those for the other channel geometries.

In summary, the following conclusions are drawn for upflow CHF in a round tube:

(1) There is a minimum in CHF at stagnant flow with the bottom end closed. The minimum CHF is calculated by equation (9) with $C = 1.66$.

(2) Low flow CHF is well correlated by conventional high-quality CHF correlations [17, 22, 23], which indicates that the CHF is attributed to liquid-film dryout.

(3) At intermediate mass velocities with a positive exit quality, there is a region where CHF is almost constant as a function of mass velocity. The flow in this region appears to be largely affected by the density-wave oscillation. The CHF decreases as the flow becomes less stable.

(4) At sufficiently high mass velocities, burnout occurs immediately after the onset of flow excursion. The CHF is slightly lower than that calculated from the condition $x_e = 0$ and is close to the subcooled-boiling CHF.

3.3.2. *Downflow.* One of the results for downflow in the round tube is shown in Fig. 10 [5]. They are also compared with several CHF correlations [15, 17, 22, 23] and equations (1), (5), (9) and (10). The summary for the CHF in downflow is as follows:

(1) In a stiff system, the downflow CHF is as much as 30% lower than the upflow high-quality CHF at very low flow rates, however, the difference disappears as the flow rate increases. This may be attributed to the effect of gravity.

(2) At intermediate mass velocities, there is a region where the CHF is almost constant as a function of mass velocity, as is the case in upflow. The CHF is lower as the flow becomes less stable. When the loop has a plenum at the top (inlet of the test section), the CHF curve moves down to the annular-flow boundary as shown in Fig. 10.

(3) At sufficiently high mass velocities, burnout occurs due to flow excursion. CHF is close to the heat flux which is calculated from the condition $x_e = 0$.

4. EFFECT OF GEOMETRY ON CHF

4.1. *Minimum CHF*

At stagnant flow with the bottom end closed or very low flow conditions, burnout due to CCFL or flooding appears to be common to all the geometries tested in this study. This type of burnout is important because it results in a minimum CHF. The minimum CHF is usually much lower than the pool-boiling CHF unless the ratio L/D_H is small. The relation between the CHF due to flooding and the pool-boiling CHF was discussed previously [3]. It was pointed out there that the CHF due to flooding increases with increasing diameter and decreasing heated length until it reaches the pool-boiling CHF.

Some variation in the burnout phenomenon due to flooding was observed between different channel geometries. In an annulus [3], falling film is formed on

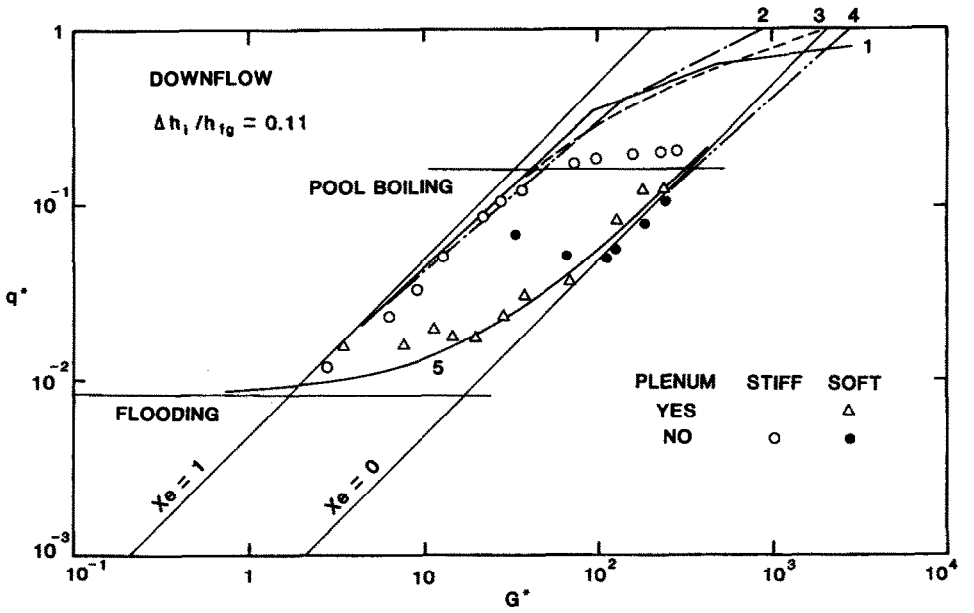

FIG. 10. CHF for downflow in a round tube [5].

both the heated and unheated walls almost uniformly, and burnout occurs when the liquid film on the heated surface dries out due to flooding. The CHF is well reproduced by equation (9) with $C = 0.98$ and by using the hydraulic equivalent diameter, i.e. $2s$ (two times the gap of the annulus) as the characteristic length. As regards to the characteristic length, there exists some disagreement among investigators. Richter [24] used the average circumference of the annulus, i.e. $(D_i + D_o)/2$, whereas Ueda and Suzuki [25] used the hydraulic equivalent diameter. Further studies are needed on this point.

In a rectangular duct with a large aspect ratio [4], the falling film is not uniform around the channel. The major portion of the liquid flows down along the narrower side walls, not along the heated wall (wider wall). As long as a sufficient amount of liquid flows along the narrower side walls, dry patches on the heated wall are quenched by the passage of large disturbance waves and lumps of liquid broken off from the liquid film. Permanent dryout of the heated surface occurs when a sufficient amount of liquid is not supplied to the heated section due to flooding. The CHF in this case is correlated using equation (9) with $2w$ (two times the channel width) as the characteristic length and $C = 0.73$.

In a round tube [5], the minimum CHF is given by equation (9) with $C = 1.66$. This value of C is much larger than those for the other channel geometries.

Equation (9) is compared with some existing data [3–5, 26–29] plotted in terms of q^*_{cF} and the parameter ζ given by

$$\zeta = \frac{A\sqrt{D^*}}{A_H[1+(\rho_g/\rho_l)^{1/4}]^2}. \tag{14}$$

Using equation (14), equation (9) can be rewritten as

$$q^*_{cF} = C^2\zeta. \tag{15}$$

The results are shown in Fig. 11. A reasonable agreement is observed between the data and equation (15).

4.2. *CHF as a function of mass velocity*

It turned out that the behavior of CHF at low and intermediate mass velocities was different between a round tube and the other geometries. Figure 12 illustrates the overall trend of CHF in a round tube. At stagnant or very low flow condition, the CHF approaches the flooding CHF. At low mass velocities, the CHF occurs due to almost complete evaporation of the liquid entering the heated section. Hence, the critical quality is close to unity, and the CHF is well reproduced by the high-quality CHF correlations. At intermediate mass velocities, there is a region where CHF becomes almost independent of the mass velocity. The CHF is lower when the flow is more unstable. The annular-flow boundary may be the lower limit of the CHF in this region, while the high-quality CHF is the upper limit. At high mass velocities, the CHF is well correlated by the subcooled-boiling CHF correlations.

On the other hand, in annuli and rectangular ducts, the overall trend of CHF appears to be as illustrated in Fig. 13. At stagnant or very low flow conditions, there appears to be no difference in the behavior of CHF between different channel geometries. At low and intermediate mass velocities, however, the effect of channel geometry becomes remarkable. The CHF stays close to the flooding CHF or the annular-flow boundary, instead of increasing along the high-quality CHF curve. The critical quality is rather small because

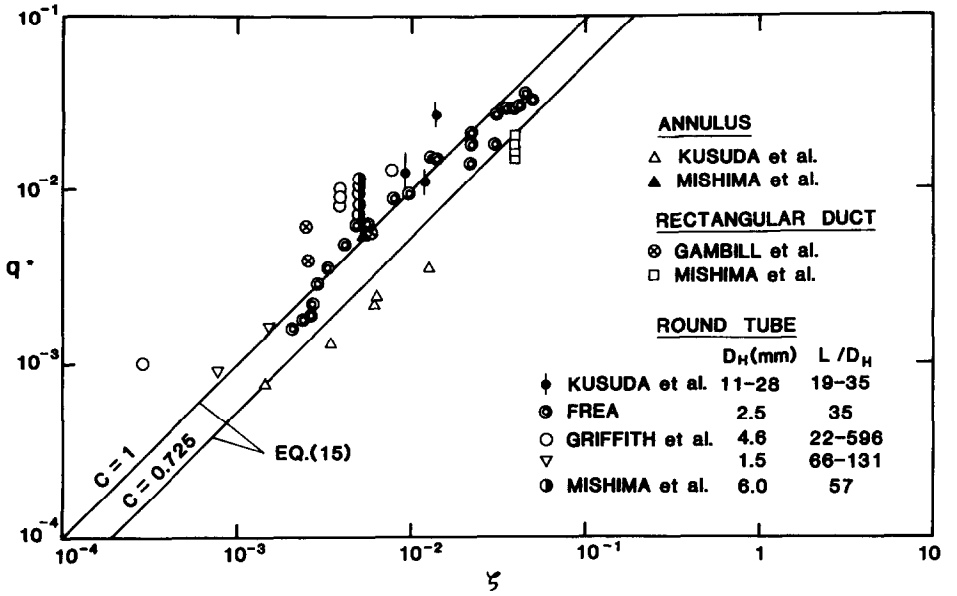

FIG. 11. Comparison between equation (15) and the data of CHF due to CCFL.

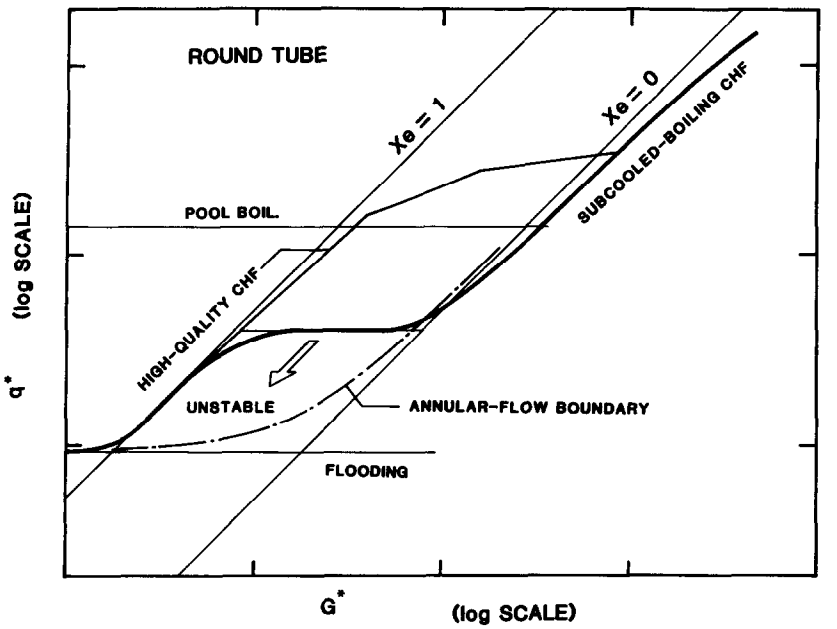

FIG. 12. Overall trend of CHF vs mass velocity for a round tube.

a substantial amount of liquid remains on the unheated wall even at CHF.

The critical quality for a channel with unheated walls, which we call a reduced critical quality, is approximated by the following equation [30]

$$x_{ec} = x_{eR}\xi_H/\xi. \tag{16}$$

Here x_{eR} is the critical quality in a round tube and can be estimated from the Katto L-regime correlations [11, 16, 22] given by

$$x_{eR} = \left(\frac{\sigma\rho_l}{G^2L}\right)^{0.043}. \tag{17}$$

Using the reduced critical quality, the modified Katto L-regime correlation can be written as

$$q^*_{cL} = \frac{A}{A_H}(x_{ec} + \Delta h_i/h_{fg})G^*. \tag{18}$$

There are some data for an annulus [31] which agree

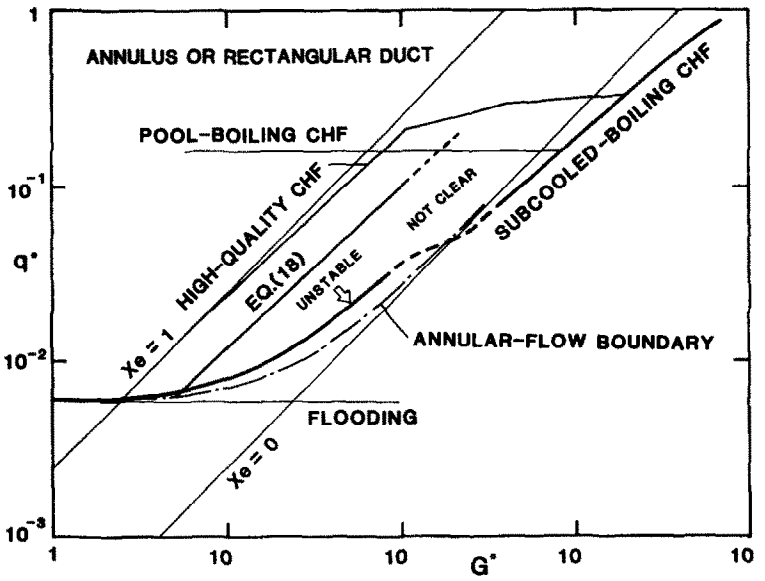

FIG. 13. Overall trend of CHF vs mass velocity for an annulus and a rectangular duct.

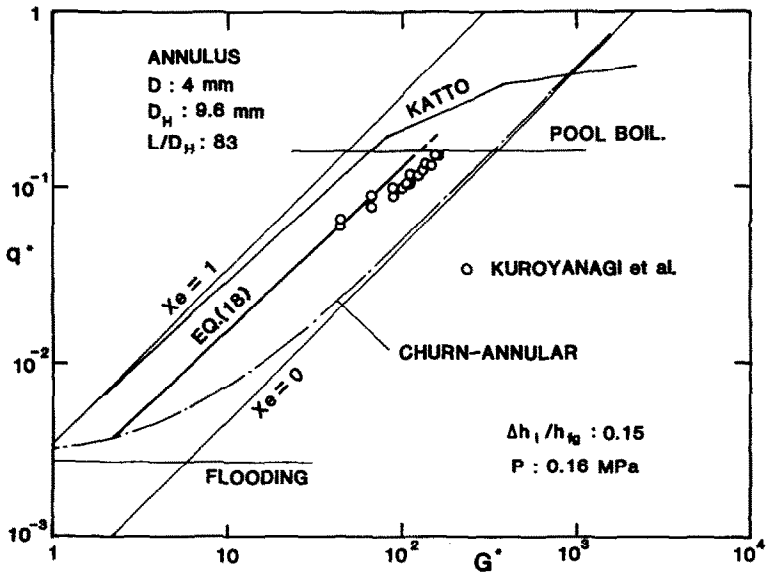

FIG. 14. Comparison between equation (18) and the data of Kuroyanagi and Iwamura [31].

reasonably well with equation (18) as shown in Fig. 14. From these results, it is deduced that the CHF for annuli lie somewhere between the curve given by the reduced critical quality and the annular-flow boundary. However, this should be limited to a low pressure system, because there are some data indicating that the Katto L-regime correlation [11] reproduces CHF data for annuli at high pressures well.

The same argument can be followed for rectangular ducts. Comparisons between CHF data for the rectangular ducts and equation (18) are given in Figs. 15 and 16. For rectangular ducts, however, the reduction of the critical quality may not be given only by the geometrical consideration of equation (16) because the liquid film on the unheated walls (narrower side walls) is much thicker than that on the heated wall. Therefore, a certain parameter would be needed to account for the effect of the non-uniform distribution of film flow for more accurate critical quality.

From the above discussions, it can be seen that the difference between different geometries in the behavior of CHF at low pressures and low mass velocities is mainly attributed to the amount of liquid flowing along the unheated wall at the occurrence of burnout.

At high mass velocities, burnout occurs when the exit quality is near zero or slightly negative. The CHF can be reproduced by the subcooled-boiling CHF cor-

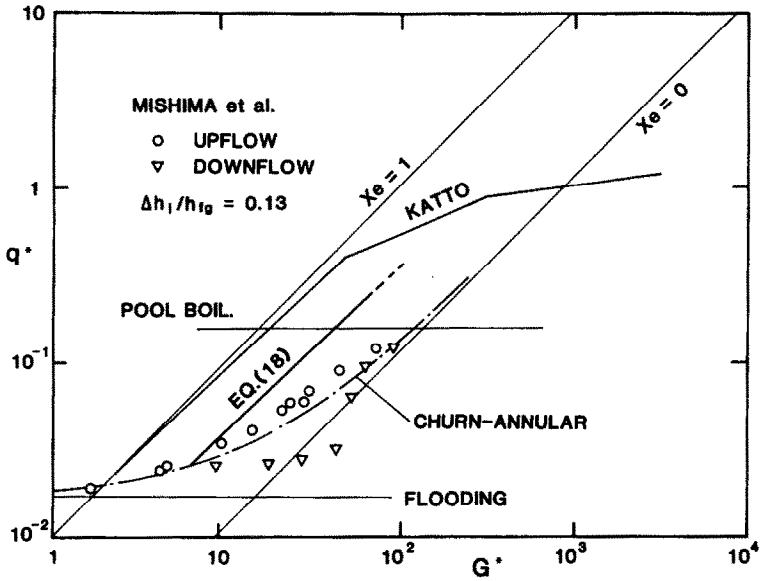

FIG. 15. Comparison between equation (18) and the previous data for the rectangular channel heated from one side [4].

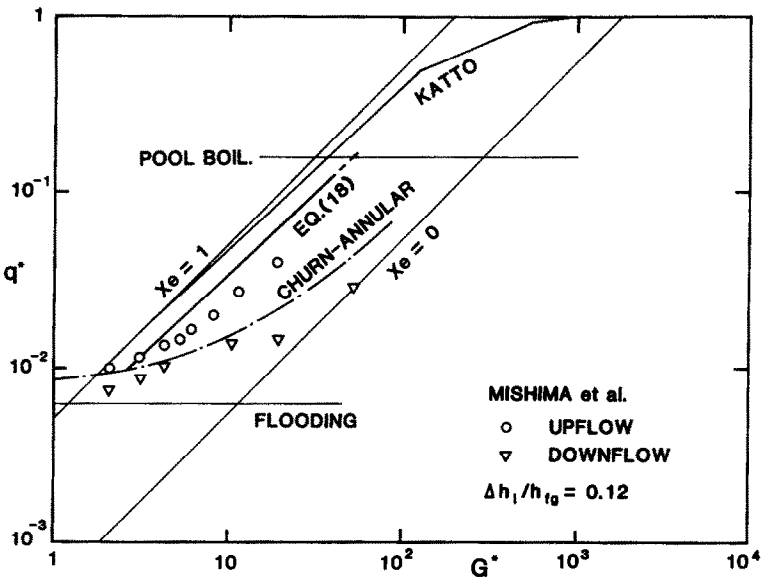

FIG. 16. Comparison between equation (18) and the previous data for the rectangular channel heated from two sides [4].

relations. Thus, the effect of channel geometry on CHF is small at high mass velocities.

5. CONCLUSIONS

The results from this study are summarized as follows:

(1) There is a minimum in CHF which occurs due to CCFL (flooding or flow reversal) at flow stagnation with the bottom end closed. If the flooding CHF is correlated by equation (9), the value of C for a round tube appears to be larger than that for an annulus and a rectangular duct.

(2) The behavior of CHF as a function of mass velocity differs between round tubes and the other channel geometries with the unheated wall at low and intermediate mass velocities. The overall trends of CHF are illustrated in Figs. 12 and 13. The difference is mainly attributed to the existence of the unheated wall. The effect of the unheated wall may be explained by using equation (16).

(3) The less stable the flow is, the lower CHF is observed at intermediate mass velocities. The upper

limit of CHF in this region is the high-quality CHF, whereas the lower limit is the flooding CHF and the condition $x_e = 0$ or the annular-flow boundary.

(4) At high mass velocities, the CHF is correlated well by the subcooled-boiling CHF correlations. The effect of channel geometry on CHF in this region appears to be small.

Acknowledgements—The authors would like to express their thanks to Professor Itaru Michiyoshi of the Department of Nuclear Engineering of Kyoto University for his invaluable comments and discussions about the subject. Thanks are also extended to Professor Toshikazu Shibata of the Research Reactor Institute of Kyoto University for his support in this work. This work was supported by the Grant-in-Aid for Scientific Research No. 59127014 (1984) from the Ministry of Education, Science and Culture of Japan.

REFERENCES

1. A. E. Bergles, Burnout in boiling heat transfer. Part III: high-quality systems, *Nucl. Safety* **20,** 671–689 (1979).
2. V. Marinelli, Critical heat flux: a review of recent publications, *Nucl. Technol.* **34,** 135–171 (1977).
3. K. Mishima and M. Ishii, Experimental study on natural convection boiling burnout in an annulus, *Proceedings of the 7th International Heat Transfer Conference*, München, Vol. 4, Paper No. FB23 (1982).
4. K. Mishima and H. Nishihara, The effect of flow direction and magnitude on CHF for low pressure water in thin rectangular channels, *Nucl. Engng Des.* **86,** 165–181 (1985).
5. K. Mishima, H. Nishihara and I. Michiyoshi, Boiling burnout and flow instabilities for water flowing in a round tube under atmospheric pressure, *Int. J. Heat Mass Transfer* **28,** 1115–1129 (1985).
6. S. S. Kutateladze, Heat transfer in condensation and boiling, AEC-tr-3770 (1959).
7. N. Zuber, Hydrodynamic aspects of boiling heat transfer, AECU-4439 (1959).
8. G. B. Wallis, Flooding velocities for air and water in vertical tubes, AEEW-R123 (1961).
9. G. B. Wallis and S. Makkenchery, The hanging film phenomenon in vertical annular two-phase flow, *J. Fluids Engng* **96,** 297–298 (1974).
10. K. Mishima and M. Ishii, Flow regime transition criteria for upward two-phase flow in vertical tubes, *Int. J. Heat Mass Transfer* **27,** 723–737 (1984).
11. Y. Katto, Generalized correlation of critical heat flux for the forced convection boiling in vertical uniformly heated annuli, *Int. J. Heat Mass Transfer* **22,** 575–584 (1979).
12. P. G. Barnett, A correlation of burnout data for uniformly heated annuli and its use for predicting burnout in uniformly heated rod bundles, AEEW-R463 (1966).
13. J. T. Rogers, M. Salcudean and A. E. Tahir, Flow boiling critical heat fluxes for water in a vertical annulus at low pressure and velocities, *Proceedings of the 7th International Heat Transfer Conference*, München, Vol. 4, Paper No. FB28 (1982).
14. F. Tachibana *et al.* (Editors), Report on burnout mechanisms: 1965 research for peaceful uses of atomic energy, JSME Report (June 15, 1967), in Japanese.
15. B. A. Zenkevich, The generalization of experimental data on critical heat fluxes in forced convection of subcooled water, *J. nucl. Energy*, Part B: *Reactor Technol.* **1,** 130–133 (1959).
16. Y. Katto, General features of CHF of forced convection boiling in uniformly heated rectangular channels, *Int. J. Heat Mass Transfer* **24,** 1413–1419 (1981).
17. R. V. Macbeth, Burnout analysis, Part 4: application of a local conditions hypothesis to world data for uniformly heated round tubes and rectangular channels, AEEW-R267 (1963).
18. S. Mirshak, W. S. Durant and R. H. Towell, Heat flux at burnout, DP-355 (1959).
19. D. A. Labuntsov, Critical thermal loads in forced motion of water which is heated to a temperature below the saturation temperature, *Soviet J. Atomic Energy* (English translation) **10,** 516–518 (1961).
20. S. S. Kutateladze, Critical thermal flow for the flow of a wetting liquid containing an underheated core, *Energetica* **2,** 229–239 (1959).
21. M. Ishii, One-dimensional drift flux model and constitutive equation for relative motion between phases in various two-phase flow regimes, ANL-77-47 (1977).
22. Y. Katto, A generalized correlation of critical heat flux for the forced convection boiling in vertical uniformly heated round tubes, *Int. J. Heat Mass Transfer* **21,** 1527–1542 (1978).
23. W. H. Lowdermilk, C. D. Lanzo and B. L. Siegel, Investigation of boiling burnout and flow stability for water flowing in tubes, NACA-TN-4382 (1958).
24. H. J. Richter, Flooding in tubes and annuli, *Int. J. Multiphase Flow* **7,** 647–658 (1981).
25. T. Ueda and S. Suzuki, Behavior of liquid films and flooding in counter-current two-phase flow. Part 2. Flow in annuli and rod bundles, *Int. J. Multiphase Flow* **4,** 157–170 (1978).
26. P. Griffith, W. A. Schumann and A. D. Neustal, Flooding and burnout in closed-end vertical tubes, *Two-phase Fluid Flow Symposium*, Paper No. 5, Inst. Mech. Engrs, London (1962).
27. H. Kusuda and H. Imura, Stability of a liquid film in a counter-current annular two-phase flow, *Bull. Japan Soc. mech. Engrs* **17,** 1613–1618 (1974).
28. W. J. Frea, Two-phase heat transfer and flooding in counter current flow, *Proceedings of the 4th International Heat Transfer Conference*, Paris, Paper No. B5.10 (1970).
29. W. R. Gambill and R. D. Bundy, Burnout heat fluxes for low-pressure water in natural circulation, ORNL-3026 (1960).
30. M. Ishii and H. K. Fauske, Boiling and dryout behavior in a liquid-metal fast breeder reactor subassembly bundle under low heat flux and low flow conditions, *Nucl. Sci. Engng* **84,** 131–146 (1983).
31. T. Kuroyanagi and T. Iwamura, Flow reduction transient burnout in an annular test section, JAERI-M8047 (1979).

EFFET DE LA GEOMETRIE DU CANAL SUR LE FLUX THERMIQUE CRITIQUE POUR L'EAU A BASSE PRESSION

Résumé—La difficulté d'interprétation du flux critique (CHF) à faible vitesse et à basse pression provient de ce que le phénomène de brûlage dans ces conditions est perturbé par les effets de convection naturelle et d'instabilité d'écoulement. Cette étude est menée pour fournir une compréhension de ce problème. Les résultats des expériences pour l'eau dans un espace annulaire, dans des canaux rectangulaires et un tube circulaire sont analysés et complétés pour extraire une information maximale. On discute l'effet de la géométrie du canal sur le CHF. Cet effet est remarquable pour des vitesses intermédiaires. La différence des CHF entre le cas d'un tube circulaire et les autres géométries est principalement attribuée à l'existence d'une paroi non chauffée qui cause une distribution non uniforme du film liquide.

DER EINFLUSS DER KANALGEOMETRIE AUF DIE KRITISCHE WÄRMESTROMDICHTE VON WASSER BEI NIEDRIGEM DRUCK

Zusammenfassung—Die Hauptschwierigkeiten bei der Beurteilung der kritischen Wärmestromdichte (CHF) bei kleinen Geschwindigkeiten und niedrigen Drücken ist die Tatsache, daß das burnout-Phänomen bei derartigen Bedingungen sehr sensibel gegen Schwerkrafteffekte und Strömungsinstabilitäten ist. Diese Studie beabsichtigt, einige grundlegende Vorstellungen über die kritische Wärmestromdichte bei kleinen Geschwindigkeiten und niedrigen Drücken zu vermitteln. Meßdaten, die in einem Ringspalt in rechteckigen Kanälen und in kreisrunden Rohren gewonnen wurden, werden in kurzer Form Gesichtet und zusammen mit vorhandenen Daten und Korrelationen gesammelt, um daraus allgemeingültigere Informationen zu erhalten. Anschließend wird der Einfluß der Kanalgeometrie auf die kritische Wärmestromdichte diskutiert. Es stellte sich heraus, daß der Einfluß der Kanalgeometrie bei mittleren Massenströmen von Bedeutung ist. Der Unterschied in der kritischen Wärmestromdichte bei diesen Massenströmen zwischen einem kreisrunden Rohr und den anderen Kanalgeometrien wurde hauptsächlich auf das Vorhandensein einer unbeheizten Wand, die eine Ungleichverteilung des Flüssigkeitsfilms bewirkt, zurückgeführt.

ВЛИЯНИЕ ГЕОМЕТРИИ КАНАЛА НА КРИТИЧЕСКИЙ ТЕПЛОВОЙ ПОТОК ДЛЯ ВОДЫ ПРИ МАЛОМ ДАВЛЕНИИ

Аннотация—Основная трудность при интерпретации критического теплового потока (КТП) при малой скорости и низком давлении состоит в том, что на КТП оказывают влияние подъемные силы и неустойчивость течения. Дан обзор исследований по течению воды в кольцевых и прямоугольных каналах и круглой трубе, которые дополнены имеющимися данными и соотношения для получения более полной информации. Обсуждается влияние геометрии канала на КТП, которое оказывается значительным при промежуточных массовых скоростях. Различия в КТП при указанных массовых скоростях в круглой трубе и в каналах другой формы связано в основном с существованием ненагретой стенки, которая вызывает неоднородное распределение пленки жидкости.